High temperature efficient, stable Si wafer-based selective solar absorbers

Hao Tian, Zhiguang Zhou, Tianran Liu, Cindy Karina, Urcan Guler, Vladimir Shalaev, and Peter Bermel

Citation: Appl. Phys. Lett. **110**, 141101 (2017); doi: 10.1063/1.4979510
View online: http://dx.doi.org/10.1063/1.4979510
View Table of Contents: http://aip.scitation.org/toc/apl/110/14
Published by the American Institute of Physics

High temperature efficient, stable Si wafer-based selective solar absorbers

Hao Tian,[1] Zhiguang Zhou,[1] Tianran Liu,[1] Cindy Karina,[2] Urcan Guler,[1] Vladimir Shalaev,[1] and Peter Bermel[1,a)]

[1]*Birck Nanotechnology Center, Electrical and Computer Engineering, 1205 W. State St, Purdue University, West Lafayette, Indiana 47907, USA*

[2]*ETH (Swiss Federal Institute of Technology) Zurich, Technopark, ETH-Building, Technoparkstr. 1, CH-8005 Zurich, Switzerland*

(Received 4 January 2017; accepted 16 March 2017; published online 3 April 2017)

Creating selective solar absorber systems using simple, stable structures capable of surviving high temperatures is essential for widespread adoption of efficient, high-temperature solar thermal technologies. In this study, semiconductor-metal tandem selective solar absorbers based on commercially available Si wafers are fabricated and measured at different high temperatures. High selectivity of the devices is obtained at temperature as high as 490 °C, and the structure is demonstrated to be mechanically and thermally stable even at slightly higher temperatures (up to 535 °C). Increased free carrier absorption and lattice absorption of Si are observed at elevated temperatures, which raise thermal re-radiation dramatically. In order to mitigate this effect, a thin Si film-based selective absorber has also been computationally designed and optimized, which is predicted to exhibit even higher thermal transfer efficiency (60–70%) at a wide range of solar concentrations (20–100 suns). The simple structure combined with the mechanical and thermal stability enables the low-cost Si substrate-based selective solar absorber to find wide applications in solar thermal energy conversion systems. *Published by AIP Publishing.* [http://dx.doi.org/10.1063/1.4979510]

The efficiency of power conversion from solar to some other usable form of energy is a key factor in the economic feasibility of processes that harvest solar energy. For medium-energy photons, particularly below 1 eV, it can in fact be most effective to use thermal conversion. However, for low-energy photons, it is best not to absorb them, to suppress infrared re-radiation. Efficient thermal capture of solar power requires high solar absorptivity of medium- to high-energy photons, as well as low thermal re-radiation at the operating temperature. A highly selective solar absorber allows one to cleanly discriminate between these wavelength ranges. Its performance can be quantified by measuring the thermal transfer efficiency η_t, which is the fraction of thermal power that can be extracted from concentrated sunlight, defined as[1]

$$\eta_t = \bar{\alpha} - \frac{\bar{\varepsilon}\sigma T^4}{CI}, \tag{1}$$

where σ is the Stefan–Boltzmann constant, T is the temperature of the selective absorber in Kelvin, C is the solar concentration, I is the solar intensity, usually given as 1 kW/m^2, $\bar{\alpha} = (1/I)\int_0^\infty d\lambda\, \varepsilon(\lambda) dI/d\lambda$ is the spectrally averaged absorptivity, $dI/d\lambda$ is the AM1.5 solar intensity per unit wavelength, and $\varepsilon(\lambda)$ is the emissivity of the selective surface. Finally, the spectrally averaged emissivity $\bar{\varepsilon}$ is given by

$$\bar{\varepsilon} = \frac{\int_0^\infty d\lambda\, \varepsilon(\lambda) \Big/ \left\{\lambda^5\left[\exp\left(\frac{hc}{\lambda kT}\right) - 1\right]\right\}}{\int_0^\infty d\lambda \Big/ \left\{\lambda^5\left[\exp\left(\frac{hc}{\lambda kT}\right) - 1\right]\right\}}, \tag{2}$$

where h is Planck's constant and k is Boltzmann's constant. High efficiency systems (e.g., solar thermophotovoltaics, solar thermoelectrics[2]) also require mechanical and thermal stability at high operating temperatures.[3] Thus, a system-level approach to the design and optimization of selective absorbers is required.

Many structures have been recently proposed and studied for selective solar absorbers such as metal-dielectric composite coatings,[4] semiconductor-metal tandems,[5–7] metamaterial surfaces,[8–10] and metallic photonic crystals.[11–16] Among them, semiconductor-metal tandem selective solar absorbers have been demonstrated to possess high thermal transfer efficiency in both the theory[17] and experiment.[5,7] Since semiconductor materials absorb most photons with energy above the bandgap and are transparent to that below the bandgap, they naturally possess spectral selectivity. A wide variety of semiconductor materials can potentially be used in this context, such as silicon (Si),[7] germanium (Ge),[18] and lead sulfide (PbS).[19] According to Kirchoff's law of thermal radiation,[20] the emissivity ε equals absorptivity α in thermodynamic equilibrium, which can be expressed by reflectivity R for opaque objects, that is $\varepsilon(\lambda) = \alpha(\lambda) = 1\text{-}R(\lambda)$. By adding a metal back reflector, long wavelength light passing through the semiconductor will be reflected, thus reducing thermal emission.[21] Since most semiconductor materials have a high refractive index, a front anti-reflection (AR) coating is also needed for maximally efficient absorption of sunlight. Compared with other selective solar absorber structures, the semiconductor-metal tandem is low-cost, easy to fabricate, and mechanically stable.

Several researchers have previously investigated related semiconductor-metal tandem structures. Donnadieu *et al.* considered a silicon/germanium tandem absorber placed on a silver reflector with a dielectric anti-reflection coating in front.[7] Numerical optimizations predict a spectrally averaged

a)Author to whom correspondence should be addressed. Electronic mail: pbermel@purdue.edu.

absorptivity $\bar{\alpha} = 0.89$ and spectrally averaged emissivity $\bar{\varepsilon} = 0.0389$ at 300 °C and $\bar{\varepsilon} = 0.0545$ at 500 °C. Okuyama *et al.* also fabricated an amorphous silicon absorber with an anti-reflection coating and aluminum reflector,[6] which was measured to have $\bar{\alpha} = 0.79$–0.81 and $\bar{\varepsilon} = 0.12$–0.14 at 400 °C. More recently, Bermel *et al.* numerically optimized crystalline silicon absorbers with silver back reflectors and anti-reflection coatings. Under 100 suns solar concentration at an absorber temperature of 1000 K, silicon actually has an appropriate bandgap, yielding $\bar{\alpha} = 0.868$ and $\bar{\varepsilon} = 0.073$, for a thermal transfer efficiency $\eta_t = 0.822$.[17] In this manuscript, we focus on selective absorbers with single-crystal Si wafers, since they are reasonably low cost and widely available, and their optical properties have been extensively studied across a broad range of temperatures. As a result, semi-empirical models of the high temperature optical property of crystalline Si have been carefully validated,[22] allowing us to accurately simulate our proposed structures. Still, given that polished multi-crystalline Si wafers are now available at even lower cost, such materials may warrant further investigation in future work.

Following up on these results, a semiconductor-metal tandem selective solar absorber based on a low-cost Si wafer is fabricated and measured at different high temperatures in this work. The structure, shown in the inset of Fig. 1, includes silicon nitride (Si_3N_4) AR coating (215 nm), and a silver (Ag) back reflector (300 nm). High selectivity is observed up to 490 °C, with thermal stability up to 535 °C. However, thermal re-radiation from silicon's intrinsic free carrier absorption at high temperatures limits the maximum operating temperature.[23] To mitigate this effect, a thin-film Si selective absorber is designed and optimized for a high η_t for solar concentrations below 100 suns.[24,25] Additionally, thin Si film substrates exhibit attractive qualities such as excellent mechanical stability and flexibility, as demonstrated by Cui *et al.*[26]

To simulate the emissivity of the proposed structure of the selective solar absorber, we employ the Stanford Stratified Structure Solver (S4),[27,28] which solves Maxwell's equations in the frequency domain with rigorous coupled wave analysis.[29] A plane wave is input at normal incidence, and the reflectance and thus emissivity at each wavelength are calculated, according to Kirchoff's law. The optical material properties are obtained from the literature. The complex refractive index of Si_3N_4 is taken from experiments by Kischkat *et al.*[30] Since it is very thin, we assume that its temperature dependence is negligible. Similarly, the complex refractive index of Ag is obtained from the study by Rakic *et al.*;[31] its temperature dependence is also neglected. However, since Si is relatively thick and has strong temperature dependence,[23] its optical properties are carefully modeled. At room temperature, we combine results from Green and Keevers,[32] Salzberg and Villa,[33] and Bermel *et al.*[17] to cover the entire wavelength range. At higher temperatures, we rely on the semi-empirical models reviewed by Roozeboom.[22] This approach allows emissivity to be precisely simulated at room temperature and beyond, for direct comparison with experimental results.

The selective solar absorber (SSA) is fabricated on a standard 300 μm, lightly N-doped, double side polished Si wafer (Pure Wafer). A 300 nm-thick silver layer is first deposited on the back of the Si wafer using a CHA e-beam evaporator at a deposition rate of 1.5 Å/s (determined by a quartz crystal monitor). The thickness is chosen to reduce the risk of agglomeration at high temperatures,[5] which would decrease the reflectance. A 215 nm Si_3N_4 AR coating is finally sputtered on the top of the Si substrate using a magnetron sputtering system (custom-built by PVD Products) with a 100 W AC power supply under 5 mTorr and 15 sccm Ar. The deposited Si_3N_4 thickness is measured by spectroscopic ellipsometry (Filmetrics).

The room temperature diffuse and specular reflectance of the SSA is measured by a PerkinElmer Lambda 950 spectrophotometer with an integrating sphere (Labsphere) for 0.5–2.5 μm, as shown in Fig. 1. This spectrum matches well with simulations, which also predict a sharp cutoff of emissivity around 1.1 μm, corresponding to the band edge of Si. This cutoff enables the selective absorber to effectively absorb most sunlight, while suppressing re-radiation for high η_t. Furthermore, as shown in Fig. 1, the AR coating effectively increases the absorptance of high-energy photons, peaking near unity at 550 nm, the maximum of the solar spectrum.

The direct thermal emissivity spectrum measurement setup for high temperatures is illustrated in Fig. 2. The sample

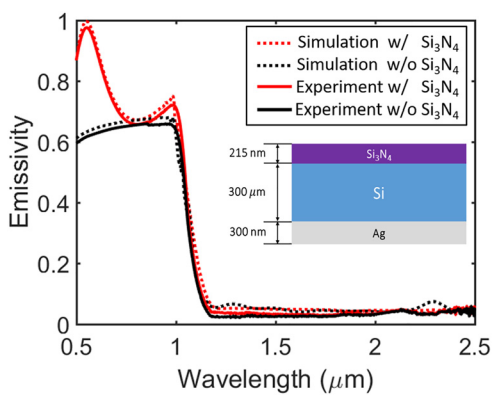

FIG. 1. Measurement (solid lines) and simulation (dashed lines) of the emissivity of selective absorbers with (red lines) and without (black lines) front AR coating at room temperature. Measurements performed by a PerkinElmer Lambda 950 spectrophotometer with an integrating sphere (Labsphere). The inset is the schematic of the structure for the selective absorber based on the Si substrate with 215 nm Si_3N_4 front anti-reflection coating (ARC) and 300 nm Ag back reflection layer. Thicknesses not to scale.

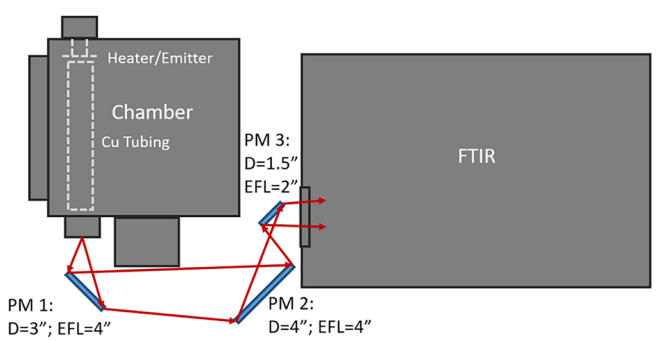

FIG. 2. Schematic of the direct thermal emission spectrum measurement system. The sample is heated by the heater, and the emitted light is collected and guided by the Cu tube. Three off-axis parabolic mirrors (PM 1, 2, and 3) are used to reflect and collimate the signal into an FTIR spectrometer. D is the diameter of the mirror, and EFL is the effective focal length of off-axis parabolic mirrors.

is heated by a proportional–integral–derivative (PID) controlled heater (HTR1001, Tectra) with direct contact and placed in a high vacuum chamber ($\sim 10^{-7}$ Torr) during the measurement. A double heat shield structure is used to block thermal emission signals from the heater. The emission signal is collected and guided by an interior polished Copper (Cu) tube inside the chamber. After transmitting through a CaF_2 window, the emission is reflected and collimated by three off-axis parabolic mirrors (PM 1, 2, and 3, Edmund Optics) to a Fourier Transform InfraRed (FTIR) spectrometer with a liquid nitrogen cooled (77 K) mercury cadmium telluride (MCT) detector paired with a KBr beam splitter (Thermo Fisher Nexus 670). A low mirror velocity (0.1581 cm/s) is chosen for a broadband scan covering 1–10 μm. An acceptable signal to noise ratio is achieved with 100 scans. A multi-wall carbon nanotube (MWCNT) sample grown on a 1 cm × 1 cm silicon wafer is used as a blackbody reference ($\bar{\alpha} = 0.96$ at room temperature).[34] To measure the surface temperature of the emitter sample, a type K thermocouple (SCASS-020U-12-SHX, Omega) is attached to the sample's surface by high-temperature paste (Ultra-temp 516, Aremco). Finally, the emissivity of the selective solar absorber is calculated using the blackbody emission and the background signals as in Ref. 35. This method results in the following emissivity equation:

$$\varepsilon(\lambda) = \frac{B \cdot \varepsilon_{CNT}(\lambda) A_{CNT}[P(\lambda, T_{CNT}) - P(\lambda, T_R)] - B \cdot \Delta A_{CNT} P(\lambda, T_R) + \Delta A_{SA} P(\lambda, T_R)}{A_{SA}[P(\lambda, T_{SA}) - P(\lambda, T_R)]}, \tag{3}$$

where

$$B = \frac{FTIR_{SA}(\lambda, T_h, T_{SA}) - FTIR_B(\lambda, T_h)}{FTIR_{CNT}(\lambda, T_h', T_{CNT}) - FTIR_B(\lambda, T_h')}. \tag{4}$$

$\varepsilon(\lambda)$ is the spectral emissivity of the emitter; the subscripts *CNT*, *SA*, *h*, and *R* stand for the MWCNT sample, selective absorber sample, heater, and room-temperature, respectively; $P(\lambda, T)$ is the blackbody radiance at temperature T; $FTIR(\lambda)$ is the spectrum measured directly by FTIR; A is the surface area of the emitter; and ΔA is the difference between the emitting area and the sample area. The nonzero ΔA is caused by the shadowing of sample mounting and the thermocouple.

The emissivity of the selective absorber with and without Si_3N_4 AR coating at different high temperatures is measured using the direct thermal emission measurement system described above, as shown in Fig. 3. Due to the surface temperature non-uniformity, thermocouple contact resistance, and measurement error of ~2%, the actual sample surface temperature differs slightly from the direct reading from the thermocouple. To more precisely estimate the surface temperature, the measured temperature should be adjusted slightly to achieve the best match between simulations and experiments. The remaining discrepancy between the theory and experiment [e.g., 515 + 20 °C in Fig. 3(a)] is mainly due to the lower signal to noise ratio at shorter wavelengths and the area differences between the sample and the blackbody reference. Additionally, during the high temperature measurements, the increase in the temperature of the MCT detector in FTIR reduces its sensitivity, which can introduce extra errors in the measurement.

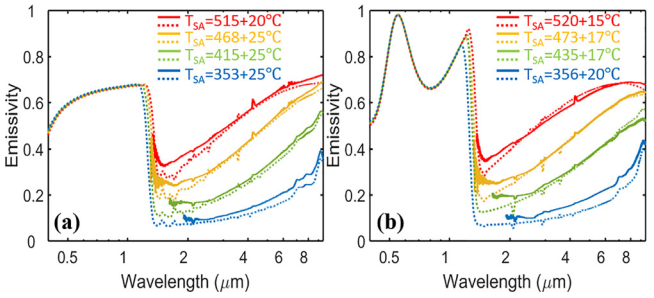

FIG. 3. Measurement (solid lines) and simulation (dashed lines) of the emissivity of the selective solar absorber: (a) without and (b) with a Si_3N_4 AR coating at different high temperatures. The thicknesses of Si_3N_4, Si, and Ag are 215 nm, 300 μm, and 300 nm, respectively, in the simulation. To account for surface temperature non-uniformity and measurement errors, corrections have been added to the measured temperature. Each curve is labelled following the format [measured temperature + correction °C]. The total number is thus the estimated actual surface temperature of the sample. High spectral selectivity is observed at 490 °C [=473 + 17 °C] for the sample with AR coating, with a cutoff wavelength of approximately 1.3 μm.

The structure with an AR coating shows increased light absorption below the cutoff at all temperatures, in contrast with the devices without front coating [Fig. 3(b)]. As expected, the cutoff wavelength redshifts to longer wavelengths with increased temperature, following the temperature dependence of the crystalline silicon band edge. As for longer wavelengths, the emissivity increases dramatically with temperature, as predicted by the model and measured in the experiment. This is mainly caused by intrinsic free carrier absorption of Si at high temperatures.[23] Also, the lattice absorption peaks around 6–9 μm are observed at relatively low temperature [353 + 25 °C and 356 + 20 °C in Figs. 3(a) and 3(b)], as predicted by the simulation. The temperature dependence of silicon's emissivity limits the temperatures at which the selective absorber can operate. Nonetheless, the Si-based solar selective absorbers show good selectivity when the temperature is as high as 490 °C [= 473 + 17 °C in Fig. 3(b)] for the sample with Si_3N_4 AR coating. Under 50 suns concentration at 490 °C, we find that $\bar{\alpha} = 0.7022$ and emissivity $\bar{\varepsilon} = 0.4877$, yielding $\eta_t = 0.5148$. After testing the SSA at high temperatures, its room temperature reflection was re-measured to characterize its degradation. Fortunately, only negligible changes in the device appearance and optical properties were observed, which is consistent with high-temperature mechanical and thermal stability.

As illustrated by the simulation and experimental results, the Si-based selective absorber is limited by strong free carrier absorption at high temperature, which increases the thermal emission and thus decreases the overall energy transfer efficiency. One possible solution for higher temperatures is to

reduce the Si thickness, to lower the mid-wavelength infrared (MWIR) re-radiation. It has recently been demonstrated that Si wafers with thicknesses below 10 μm exhibit excellent mechanical stability and bendability.[26] The simulated emissivity spectrum of thin selective Si absorbers with optimized Si_3N_4 anti-reflection coating thickness (80 nm) is compared with that of 300 μm-thick Si wafers in Fig. 4(a). Also, since Ag and Si_3N_4 have already been experimentally demonstrated to be thermally stable at temperatures above 500 °C, the temperature in the simulation is set to 550 °C.

It is clearly shown in Fig. 4(a) that the emissivity above the cutoff wavelength decreases rapidly with Si thickness, which indicates the effective suppression of free carrier absorption. Also, the selectivity maintains its sharpness across all Si thicknesses considered. Nonetheless, the cutoff wavelength blue shifts with decreasing Si thickness, because of incomplete absorption near the Si band edge. Thus, for each set of operating conditions, there is an optimal trade-off between free carrier absorption and full solar absorption. To quantitatively evaluate the performance of the selective absorber with different Si thicknesses, the dependence of η_t on solar concentration is examined across various Si thicknesses in Fig. 4(b). This calculation shows that thinner Si films are less sensitive to concentration from efficient suppression of thermal re-radiation. Thus, as solar concentration decreases, the optimal Si thickness also decreases. For concentrations as low as 20 suns, the maximum η_t for 5 μm and 10 μm Si can still be ~60%. Therefore, the low thermal emission helps maintain η_t across a broad range of concentrations (20–100 suns). Finally, note that only a single-layer anti-reflection coating was considered, so η_t might be even further increased by a multi-layer AR coating.[17]

In conclusion, a semiconductor-metal tandem selective solar absorber (SSA) has been fabricated on a low-cost Si wafer, which exhibits high selectivity and stability at high temperatures (up to 530 °C) in experiments. However, the intrinsic free carrier absorption of Si wafers limits the maximum temperature at which $\eta_t > 0.5$ for 50 suns concentration. To further suppress thermal re-radiation and improve the overall performance, we investigate the effects of reducing the Si thickness below 20 μm, and re-optimize the Si_3N_4 AR coating. We show that structures with 5 μm and 10 μm-thick Si should maintain relatively high efficiency (60–70%) at concentrations as low as 20 suns. The excellent mechanical stability previously demonstrated for thin Si films increases the likelihood of success, thus warranting further investigation.

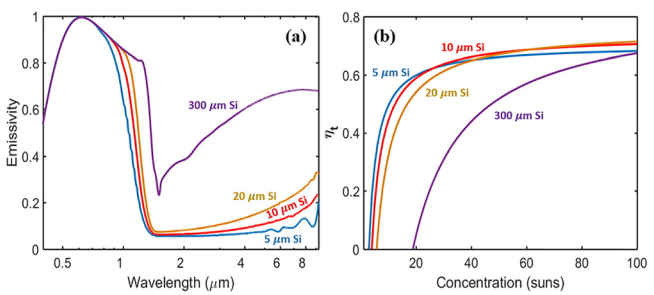

FIG. 4. (a) Simulated emissivity for selective absorbers with different Si thicknesses. The Fabry-Pérot interference around the Mid-IR is smoothed out for more clear comparison. Less MWIR absorption is experienced for thinner layers of silicon because all samples are in the intrinsic regime, and free carrier absorption dominates. (b) Dependency of the solar thermal transfer efficiency η_t on the concentration for different Si thicknesses. Thinner layers of silicon experience less re-radiation; however, layers which are too thin have less absorption, which puts an upper bound on η_t (e.g., 5 μm Si). An optimal 80 nm Si_3N_4 thickness is used for each curve, along with a temperature of 550 °C.

The authors thank Yi Cui, Hye Ryoung Lee, and Thomas Hymel for valuable discussions and thank Menglong Hao and Tim Fisher for their provision of a blackbody reference sample made from multi-wall carbon nanotubes. Support was provided by the Department of Energy, under DOE Cooperative Agreement No. DE-EE0004946 (PVMI Bay Area PV Consortium), the Semiconductor Research Corporation, under Research Task No. 2110.006 (Network for Photovoltaic Technologies), and the U.S. National Science Foundation (NSF), under Award EEC1454315-CAREER: Thermophotonics for Efficient Harvesting of Waste Heat as Electricity. Computational resources on nanoHUB.org were provided by the Network for Computational Nanotechnology, which was funded by NSF under Grant No. EEC-1227110.

[1]P. Bermel, J. Lee, J. D. Joannopoulos, I. Celanovic, and M. Soljacic, Annu. Rev. Heat Transfer **15**, 231 (2012).
[2]D. Kraemer, B. Poudel, H. Feng, J. C. Caylor, B. Yu, X. Yan, Y. Ma, X. Wang, D. Wang, A. Muto, K. McEnaney, M. Chiesa, Z. Ren, and G. Chen, Nat. Mater. **10**, 532 (2011).
[3]E. Rephaeli and S. Fan, Opt. Express **17**, 15145 (2009).
[4]T. Sathiaraj, T. Stephen, R. Thangaraj, H. Al Sharbaty, M. Bhatnagar, and O. P. Agnihotri, Thin Solid Films **190**, 241 (1990).
[5]B. O. Seraphin, Thin Solid Films **39**, 87 (1976).
[6]M. Okuyama, K. Saji, T. Adachi, H. Okamoto, and Y. Hamakawa, Sol. Energy Mater. **3**, 405 (1980).
[7]A. Donnadieu and B. O. Seraphin, J. Opt. Soc. Am. **68**, 292 (1978).
[8]C. Wu, I. I. I. B. Neuner, G. Shvets, J. John, A. Milder, B. Zollars, and S. Savoy, Phys. Rev. B **84**, 75102 (2011).
[9]C. Wu, B. Neuner III, J. John, A. Milder, B. Zollars, S. Savoy, and G. Shvets, J. Opt. **14**, 24005 (2012).
[10]H. Wang and L. Wang, Opt. Express **21**, A1078 (2013).
[11]J. B. Chou, Y. X. Yeng, A. Lenert, V. Rinnerbauer, I. Celanovic, M. Soljačić, E. N. Wang, and S.-G. Kim, Opt. Express **22**, A144 (2014).
[12]Z. Zhou, O. Yehia, and P. Bermel, J. Nanophotonics **10**, 16014 (2016).
[13]Z. Zhou, E. Sakr, O. Yehia, A. Mathur, and P. Bermel, MRS Adv. **1**, 59 (2016).
[14]J. M. Gee, J. B. Moreno, S.-Y. Lin, and J. G. Fleming, in *Conference Record of IEEE Twenty-Ninth Photovoltic Specialists Conference* (2002), pp. 896–899.
[15]I. Celanovic, N. Jovanovic, and J. Kassakian, Appl. Phys. Lett. **92**, 193101 (2008).
[16]V. Rinnerbauer, S. Ndao, Y. X. Yeng, W. R. Chan, J. J. Senkevich, J. D. Joannopoulos, M. Soljačić, and I. Celanovic, Energy Environ. Sci. **5**, 8815 (2012).
[17]P. Bermel, M. Ghebrebrhan, W. Chan, Y. X. Yeng, M. Araghchini, R. Hamam, C. H. Marton, K. F. Jensen, M. Soljačić, J. D. Joannopoulos *et al.*, Opt. Express **18**, A314 (2010).
[18]L. R. Gilbert, R. Messier, and R. Roy, Thin Solid Films **54**, 149 (1978).
[19]D. M. Mattox and G. J. Kominiak, J. Vac. Sci. Technol. **12**, 182 (1975).
[20]G. B. Rybicki and A. P. Lightman, *Radiative Processes in Astrophysics* (Wiley-VCH Verlag GmbH, Weinheim, Germany, 1985).
[21]Z. Zhou, E. Sakr, Y. Sun, and P. Bermel, Nanophotonics **5**, 1 (2016).
[22]F. Roozeboom, *Advances in Rapid Thermal and Integrated Processing* (Springer Science & Business Media, 2013).
[23]T. Sato, Jpn. J. Appl. Phys., Part 1 **6**, 339 (1967).
[24]J. I. Gittleman, E. K. Sichel, H. W. Lehmann, and R. Widmer, Appl. Phys. Lett. **35**, 742 (1979).
[25]H. G. Craighead, R. E. Howard, and D. M. Tennant, Appl. Phys. Lett. **37**, 653 (1980).

[26]S. Wang, B. D. Weil, Y. Li, K. X. Wang, E. Garnett, S. Fan, and Y. Cui, Nano Lett. **13**, 4393 (2013).
[27]V. Liu and S. Fan, Comput. Phys. Commun. **183**, 2233 (2012).
[28]J. Kang, X. Wang, P. Bermel, and C. Liu, S4: Stanford Stratified Structure Solver (2014), https://nanohub.org/resources/s4sim.
[29]E. S. Sakr, Z. Zhou, and P. Bermel, Appl. Phys. Lett. **105**, 111107 (2014).
[30]J. Kischkat, S. Peters, B. Gruska, M. Semtsiv, M. Chashnikova, M. Klinkmüller, O. Fedosenko, S. Machulik, A. Aleksandrova, G. Monastyrskyi *et al*., Appl. Opt. **51**, 6789 (2012).
[31]A. Rakic, A. Djurisic, J. Elazar, and M. Majewski, Appl. Opt. **37**, 5271 (1998).
[32]M. A. Green and M. J. Keevers, Prog. Photovoltaics Res. Appl. **3**, 189 (1995).
[33]C. D. Salzberg and J. J. Villa, J. Opt. Soc. Am. **47**, 244 (1957).
[34]J. Zuidema, X. Ruan, and T. S. Fisher, Opt. Express **21**, 22053 (2013).
[35]F. Marquier, K. Joulain, J.-P. Mulet, R. Carminati, J.-J. Greffet, and Y. Chen, Phys. Rev. B **69**, 155412 (2004).